Furukawa A, Okamura H, Morishita R, Matsunaga S, Kobayashi N, Ikegami T, Kodaki T, Takaori-Kondo A, Ryo A, Nagata T, Katahira M.	NMR study of xenotropic murine leukemia virus-related virus protease in a complex with amprenavir.	Biochem Biophys Res Commun	425 (2)	284-89	2012
Narita Y, Murata T, Ryo A, Kawashima D, Sugimoto A, Kanda T, Kimura H, Tsurumi T.	Pin1 interacts with the Epstein-Barr virus DNA polymerase catalytic subunit and regulates viral DNA replication.	J Virol	87 (4)	2120-27	2012
Ichiyama K, Gopala Reddy SB, Zhang LF, Chin WX, Muschin T, Heinig L, Suzuki Y, Nanjundappa H, Yoshinaka Y, Ryo A, Nomura N, Ooi EE, Vasudevan SG, Yoshida T, Yamamoto N.	Sulfated polysaccharide, curdlan sulfate, efficientl y prevents entry/fusion and restricts antibody-dependent enhancement of dengue virus infection in vitro: a possible candidate for clinical application.	PLoS Negl Trop Dis	7 (4)	e2188	2013
Furukawa, A., Sugase, K., Morishita, R., Nagata, T., Kodaki, T., Takaori, A., Ryo, A., Katahira, M.	Quantitative analysis of the location- and sequence-dependent deamination by APOBEC3G using real-time NMR.	Angew. Chem., Int. Ed	In press		2014
Yamada Y, Tomaru U, Ishizu A, Kiuchi T, Marukawa K, Matsuno Y, Kasahara M.	Expression of proteasome subunit β5t in thymic epithelial tumors.	Am J Surg Pathol	35 (9)	1296-1304	2011
Sutoh Y, Kondo M, Ohta Y, Ota T, Tomaru U, Flajnik MF, Kasahara M.	Comparative genomic analysis of the proteasome β5t subunit gene: implications for the origin and evolution of thymoproteasomes.	Immunogenetics	64 (1)	49-58	2012
Tomaru U, Takahashi S, Ishizu A, Miyatake Y, Gohda A, Suzuki S, Ono A, Ohara J, Baba T, Murata S, Tanaka K, Kasahara M.	Decreased proteasomal activity causes age-related phenotypes and promotes the development of metabolic abnormalities.	Am J Pathol	180 (3)	963-972	2012
Tomaru U, Yamada Y, Ishizu A, Kuroda T, Matsuno Y, Kasahara M.	Proteasome subunit β5t expression in cervical ectopic thymoma.	J Clin Pathol	65 (9)	858-859	2012

Ando H, Sato T, Tomaru U, Yoshida M, Utsunomiya A, Yamauchi J, Araya N, Yagishita N, Coler-Reilly A, Shimizu Y, Yudoh K, Hasegawa Y, Nishioka K, Nakajima T, Jacobson S, Yamano Y.	Positive feedback loop via astrocytes causes chronic inflammation in virus-associated myelopathy.	Brain	136 (Pt 9)	2876-2887	2013
Tomaru U, Kasahara M.	Thymoproteasome: role in thymic selection and clinical significance as a diagnostic marker for thymic epithelial tumors.	Arch Immunol Ther Exp (Warsz)	61(5)	357-365	2013
Miyatake Y, Oliveira AL, Jarboui MA, Ota S, Tomaru U, Teshima T, Hall WW, Kasahara M.	Protective roles of epithelial cells in the survival of adult T-cell leukemia/lymphoma cells	Am J Pathol	182 (5)	1832-1842	2013
Yamada Y, Tomaru U, Ishizu A, Kiuchi T, Kasahara M, Matsuno Y.	Expression of thymoproteasome subunit β5t in type AB thymoma.	J Clin Pathol	67(3)	276-278	2014
Ströbel P, Hartmann E, Rosenwald A, Kalla J, Ott G, Friedel G, Schalke B, Kasahara M, Tomaru U, Marx A.	Corticomedullary differentiation and maturational arrest in thymomas.	Histopathology	64(4)	557-566	2014
Tanaka M, Nitta T, Sun B, Fujisawa J, Miwa M	The route of primary HTLV-1 infection regulates HTLV-1 distribution in reservoir organs of infected mice.	Exp Thr Med.	2	89-94	2011
Tsuda M*, Tanaka M*, Mushiake M, Takahashi J, Tanaka K, Watase J, Fujisawa JI, Miwa M. *:equal contributor.	Novel path way of centrosome amplification that does not require DNA lesions.	Cancer Sci.	103	191-196	2012
T Tezuka K, Xun R, Tei M, Ueno T, Tanaka M, Takenouchi N, Fujisawa J.	An animal model of adult T-cell leulemia: humanized mice with HTLV-1-specific immunity.	Blood.	123	346-55	2014

III. 研究成果の刊行物・別刷

frontiers in
MICROBIOLOGY

ORIGINAL RESEARCH ARTICLE
published: 26 November 2013
doi: 10.3389/fmicb.2013.00346

Development of oligomannose-coated liposome-based nasal vaccine against human parainfluenza virus type 3

Kyosuke Senchi[1], Satoko Matsunaga[1], Hideki Hasegawa[2], Hirokazu Kimura[3] and Akihide Ryo[1]*

[1] Department of Microbiology, Yokohama City University School of Medicine, Yokohama, Kanagawa, Japan
[2] Department of Pathology, National Institute of Infectious Diseases, Tokyo, Japan
[3] Infectious Disease Surveillance Center, National Institute of Infectious Diseases, Tokyo, Japan

Edited by:
Hironori Sato, National Institute of Infectious Diseases, Japan

Reviewed by:
Komei Shirabe, Yamaguchi Prefectural Institute of Public Health and Environment, Japan
Ichiro Aoki, Yokohama City University School of Medicine, Japan

***Correspondence:**
Akihide Ryo, Department of Microbiology, Yokohama City University School of Medicine, 3-9 Fuku-ura, Kanazawa-ku, Yokohama, Kanagawa 236-0004, Japan
e-mail: aryo@yokohama-cu.ac.jp

Human parainfluenza viruses (HPIVs) are the etiologic agents of lower respiratory infections and pneumonia in infants, young children and immunocompromised hosts. The overarching goal for the prevention of HPIV infection is the development of an effective vaccine against HPIVs. In the present study, we investigated the effectiveness of oligomannose-coated liposomes (OMLs) as an antigen-delivery system in combination with a synthetic double-stranded RNA analog for the induction of mucosal and systematic immunity against HPIV3. Full-length hemagglutinin-neuraminidase (HN) protein was synthesized using the wheat germ cell-free protein production system and then encapsulated into OML to serve as the antigen. Intranasal administration of the HN-filling OML (OML-HN) with the synthetic double-stranded RNA adjuvant, polyriboinosinic-polyribocytidylic acid [poly(I:C)] generated significant viral-specific systemic and mucosal immune responses as evidenced by the prominent induction of serum IgG and nasal wash IgA, respectively. On the other hand, no significant immune responses were observed in mice immunized with OML-HN without the adjuvant. Furthermore, serum from mice immunized with OML-HN plus poly(I:C) significantly suppressed viral infection in cell culture model. Our results provide the first evidence that intranasal co-administration of OML-encapsulated HN with the poly(I:C) adjuvant augments the viral-specific immunity against HPIV3.

Keywords: HPIV3, HN, vaccine, oligomannose-coated liposome, adjuvant

INTRODUCTION

Human parainfluenza viruses (HPIVs) belong to the Paramyxoviridae family and are one of the major causes of acute respiratory infections (ARIs) and asthma in infants and young children (<5 years old). HPIVs were classified into four serotypes including HPIV1-4 (Henrickson, 2003; Mizuta et al., 2011). In particular, human parainfluenza virus type 3 (HPIV3) is an important infectious agent, second only to respiratory syncytial virus (RSV), that causes bronchiolitis and pneumonia in infants (Glezen et al., 1984; Counihan et al., 2001; Belshe et al., 2004; Schmidt, 2011). Therefore, the development of a practical vaccine that can prohibit HPIV3 infection in infants is urgently needed.

Currently, there is no prophylactic human vaccine against HPIV3 infection. Several previous studies employed attenuated viruses or recombinant viruses for vaccination by intranasal administration (Haller et al., 2000; Karron et al., 2011; Schmidt et al., 2011; Mason et al., 2013). The HPIV3 cp45 is a practical nasal vaccine that is derived from the JS wild-type strain of HPIV3 through 45 passages in African green monkey cells at a low temperature. This vaccine has been evaluated in clinical human trials and is known to induce the hemagglutination-inhibiting (HAI) antibody in seronegative children (Skiadopoulos et al., 1999; Karron et al., 2003; Belshe et al., 2004). The rB/HPIV3b vaccine is a cDNA-derived chimeric HPIV3 in which the genomic cDNA is partially recombined with bovine PIV3 (BPIV3); the hemagglutinin-neuraminidase (HN) and F genes from HPIV3 fused with BPIV3 whole genome (Schmidt et al., 2001; Karron et al., 2012). The rB/HPIV3 vaccine was shown to induce significantly higher titers of HAI antibodies against HPIV3 in seronegative children. A major limitation of these vaccines is their potential to cause actual infection diseases in children or immunocompromised hosts because they are live attenuated vaccines. Therefore, it is necessary to develop a safer HPIV3 vaccine with lower risks for infection that will be useful for infants and young children in clinics. In this regard, component vaccines are desirable because they use non-infectious viral subunit proteins as antigens. A previous report demonstrated the efficacy of subunit vaccines that target the HPIV3 HN and F proteins in an animal model (Ray et al., 1988). Other reports also demonstrated the induction of protective antibodies that prohibit HPIV3 infection in response to subunit vaccines that target HPIV3 antigens (Morein et al., 1983; Ray et al., 1985; Ambrose et al., 1991; Brideau et al., 1993). A caveat of subunit-based vaccination strategies is their requirement for large amounts of antigens, thus rendering them costly to produce. Therefore, it is important to develop an effective subunit vaccine that utilizes lower quantities of antigen.

To circumvent the aforementioned problems, oligomannose-coated liposome (OML) was used as a natural and non-toxic antigen-delivery system. OML efficiently targets proteins to antigen presenting cells (APCs), such as macrophages or dendritic cells (Shimizu et al., 2007; Nishimura et al., 2013). Furthermore, previous reports showed that antigens incorporated into OML were efficiently delivered to APCs by intranasal administration (de Haan

et al., 1995; Ishii and Kojima, 2010; Giddam et al., 2012). The effect of OML was shown to be relatively ineffective at inducing humoral immunity, while it preferentially activated cell-mediated immunity via cytotoxic T lymphocytes (CTLs). Therefore, for optimal induction of both humoral and mucosal immunity it is necessary to use vaccination strategies that combine OML with other adjuvant systems.

Herein, we sought to utilize OML in combination with an adjuvant double-stranded RNA polyinosinic-polycytidylic acid [Poly(I:C)] for the induction of effective humoral and mucosal immunity against HPIV3. The overarching goal was to establish a vaccination strategy that required a small amount of antigen and a few doses. Poly(I:C) is an effective adjuvant for antibody and multi-functional CD4+ T cell responses against viral infection. Poly(I:C) was shown to be an effective mucosal adjuvant for the development of antigen-specific immunity even when hosts were immunized with a relatively small quantity of antigen (Ichinohe et al., 2005; Hasegawa et al., 2009). In addition, we also took advantage of the wheat germ cell-free protein production system to synthesize our antigen, full-length HPIV3-HN protein (Takai et al., 2010). Our results highlight the utility of combining sophisticated systems in the development of a novel vaccine against HPIV3.

MATERIALS AND METHODS

CONSTRUCTION OF WHEAT CELL-FREE EXPRESSION VECTOR

HPIV3 (C243) cDNA was kindly provided by Dr. Tsukakoshi. The HN fragment was amplified by PCR using the primers BamHI-HN F (5′-GAGAGGATCCCATGGAATACTGGAAGCAT) and NotI-HN R (5′-GAGAGCGGCCGCTTAACTGCAGCTTTTTGGA). The amplified fragment was digested with BamHI and NotI and cloned into either pEU-His or pEU-GST vectors that were previously digested with the same enzymes. GST-tagged HPIV3-HN (GST-HN) construct was mutated using the reagents of a PrimeSTAR Mutagenesis Basal Kit (TakaraBio, Otsu, Japan) according to the manufacturer's instructions.

CELL-FREE PROTEIN SYNTHESIS AND PURIFICATION

In vitro transcription and cell-free protein synthesis were performed as described (Takai et al., 2010). The bilayer translation method was used to synthesize His-tagged HPIV3-HN (His-HN) protein using wheat germ extract that was optimized for Ni-affinity purification (WEPRO 7240H; Cellfree Sciences, Yokohama, Japan) and a robotic synthesizer (Protemist XE; Cellfree Sciences) according to the manufacturer's instructions. The cell-free translation reaction (15 ml) was separated into soluble and insoluble fractions by centrifuged at 15000 rpm for 15 min. The insoluble fraction was lysed using 8M Urea at room temperature for 6 h and then mixed with Ni-sepharose High Permormance beads (GE Helthcare, Hino, Japan) in the presence of 20 mM imidazole. The beads were washed three times with washing buffer (20 mM Tris–HCl, pH 7.5, 500 mM NaCl) containing 40 mM imidazole. The His-HN protein was then eluted using washing buffer containing 8M Urea, 500 mM imidazole. Purified His-HN proteins were concentrated approximately 10–20-fold using Amicon Ultra Centrifugal Filters (Merck Millipore, Billerica, MA, USA). Full-length GST-HN protein and GST-HN deletion mutant proteins synthesized using wheat germ extract optimized for GST-affinity purification (WEPRO 1240G; Cellfree Science) according to the manufacturer's instructions. Quantification of synthesized proteins was performed by densitometric scanning of the Coomassie Brilliant Blue® (CBB)-stained bands.

PREPARATION OF LIPOSOMES

Liposomes were prepared as described previously (Giddam et al., 2012; Nishimura et al., 2013). Briefly, a chloroform:methanol (2:1, *v/v*) solution containing 1.5 μmol of DPPC, 1.5 μmol of cholesterol and varying amounts of Man3-DPPE (0.15–0.0015 μmol) was added to a flask and evaporated to prepare a lipid film. PBS containing 1 or 0.5 mg/ml of full-length HPIV3-HN protein was added to the dried lipid film and multi-lamellar vesicles were prepared by intense vortex dispersion. The vesicles were extruded 10 times through a 1 μm pore polycarbonate membrane (Nucleopore, Pleasanton, CA, USA). The amount of entrapped protein was measured using a Modified Lowry Protein Assay Kit (Pierce, Rockford, IL, USA) in the presence of 0.3% (*w/v*) sodium dodecyl sulfate using HN as the standard. The particle size of the liposomes was determined using a dynamic light scattering particle size analyzer (BioMedCore Inc., Yokohama, Japan).

IMMUNIZATION OF MICE

Female BALB/c mice (Japan SLC Inc., Hamamatsu, Japan), age 6–8 weeks at the time of immunization, were used in all of the experiments. All animal experiments were carried out in accordance with the Guides for Animal Experiments Performed at Yokohama City University (YCU) and approved by the International Animal Care and Use Committee of YCU. Three to six mice for each experimental group were anesthetized with isoflurane prior to being immunized. For the primary immunization, 13 μl of single-shot mixtures were prepared as containing OML-HN (0.1 or 1.0 μg) and/or poly(I:C) (10 μg), and administered 6.5 μl of mixtures into each nostril. Three weeks later, the secondary immunization was administered in the same manner. Two weeks after the secondary immunization, as tertiary immunization, 16 μl single-shot mixtures were prepared as containing OML-HN (0.2 or 2.0 μg) and/or Poly(I:C) (10 μg), and administered 8.0 μl of mixtures into each nostril.

ENZYME-LINKED IMMUNOSORBENT ASSAY

Serum was collected on days 7 and 14 after the secondary immunization and on days 7, 14, 21, and 28 after the tertiary immunization. On day 28 after the third immunization, all of the mice were sacrificed and nasal wash fluid was collected by washing the nasal cavity of the excised head with 1 ml of PBS(-) containing 0.1% BSA. The levels of IgG and IgA antibodies against HPIV3-HN in the serum and nasal wash fluid were determined by enzyme-linked immunosorbent assay (ELISA) as described previously. Briefly, ELISA was conducted sequentially from the solid phase (Anti-GST coated 96-well plate; Thermo, Waltham, USA) with a ladder of reagents consisting of the following: (1) GST-HN protein and GST protein as a control; (2) serum or nasal wash fluid; (3) either anti-mouse IgG antibody-conjugated HRP (1:10000, Thermo) or anti-mouse IgA antibody-conjugated HRP (1:10000, BETHYL, Montgomery, TX,

USA); (4) TMB substrate buffer (Thermo); and (5) 2M sulfuric acid. The chromogen produced was measured by determining the absorbance at 450 nm with an ELISA reader. The relative levels of IgG and IgA antibodies against HN were determined relative values calculated as follows; Relative values = mean value in immunized vaccine group/mean value in immunized OML-empty group. Each values were normalized with the optic values to GST protein.

IMMUNOBLOTTING

Using standard immunoblotting methods, the presence of HN-specific IgG was detected using pooled serum from each group of mice and incubated with anti-mouse IgG HRP-conjugated secondary Ab (Thrmo) at a dilution of 1:10000 in TBST. Immobilon was used for detection (Merck Millipore).

QUANTITATIVE REAL-TIME PCR

We performed an infection inhibitor assay by mouse serum using immortalized MRC5 cells (pNifty cells). pNifty cells were seeded in 24-well plates at a concentration of 2.5×10^5 cells per well, and after 12 h the cells were infected with pre-incubated HPIV3 virus (10^7TCID$_{50}$) with or without 5 μl mouse serum in 200 μl DMEM supplemented with 5% fetal bovine serum (FBS) and 1% penicillin and streptomycin (PS). At 4 h post-infection, the cells were washed and replaced in 200 μl of DMEM containing 10% FBS and 1% PS. At 48 h after medium change, the cells were washed with PBS and total RNA was extracted using the RNeasy Mini Kit (QIAGEN, Hilden, Germany) according to the manufacturer's protocol. cDNA was synthesized using a cDNA synthesis kit (Toyobo, Osaka, Japan) and subjected to RT-PCR analysis with the SYBR Premix Ex gent Kit TaqII (Takara Bio) using an Applied Biosystems 7300 real-time PCR System. The primer sets used were as follows: HPIV3, 5′-CTCGAGGTTGTCAGGATATAG-3′ and 5′-CTTTGGGAGTTGAACACAGTT-3′; mGAPDH, 5′-CCATGGAGAAGGCTGGGG-3′ and 5′-CAAAGTTGTCATGGATGACC-3′.

RESULTS

GENERATION OF OML VACCINE AGAINST HPIV3-HN

To produce the full-length HPIV3-HN antigen, we subcloned full-length HN cDNA into two different cell-free expression vectors, pEU-His and pEU-GST for the expression of N-terminally His-tagged or GST-tagged fusion proteins, respectively (**Figure 1A**). We found that both His-HN and GST-HN proteins were efficiently synthesized using the wheat germ cell-free system (**Figures 1B,C**). His-HN proteins precipitated into the insoluble fraction (**Figure 1B**) were purified using Ni-sepharose beads in the presence of 8M Urea. GST-HN proteins were purified using glutathione sepharose beads in a regular buffer (**Figure 1C**).

After the large scale preparation of His-HN, the protein was incorporated into OML (**Figure 1D**). The particle diameter of HN-filling OML (OML-HN) and empty OML were 882 and 519 nm, respectively. The amount of carrier HN protein was approximately 32 mg per 1 mg cholesterol (**Figure 1E**) and the molar ratio of enclosed-OML to non-enclosed OML was found to be approximately 7:3 (data not shown).

IMMUNIZATION OF MICE WITH OML-HN

We investigated whether intranasal administration of OML-HN could induce a humoral immune response against the HN. **Figure 2A** depicts the time course for the immunizations and blood collection from the immunized mice. Mice were immunized intranasally with OML-HN (1 or 0.1 μg) with or without Poly(I:C), OML with or without Poly(I:C), Poly(I:C) only, or PBS. One week after the third immunization, HN-specific serum IgG was detected in mice immunized with OML-HN (1 μg) plus Poly(I:C). The serum IgG levels were increased between days 7 and 14 and reached the peak at 21 days after the final immunization. Mice immunized with the lower amount of OML-HN (0.1 μg) plus Poly(I:C) also produced HN-specific serum IgG at 28 days after the last immunization (**Figure 2B**). In contrast, there was no significant HN-specific serum IgG in mice immunized with OML-HN without Poly(I:C) or the other negative control groups (**Figure 2B**).

We next measured the levels of serum IgG and nasal wash IgA in each individual mouse by ELISA and immunoblotting (**Figures 3A–C**). Mice immunized with OML-HN (1 μg) plus Poly(I:C) exhibited prominent induction of HN-specific IgG (**Figures 3A,C**). HN-specific IgA in nasal wash fluid was most prominently induced in mice with OML-HN (1 μg) plus Poly(I:C) compared to other groups (**Figure 3B**). Interestingly, the induction of the HN-specific IgA was higher in mice that were immunized with the lower amount of antigens, OML-HN (0.1 μg) plus Poly(I:C) (**Figure 3B**).

EPITOPE MAPPING OF INDUCED ANTIBODIES

We next determined the region of HN that was recognized by the HN-specific serum IgG produced by the mice that were immunized with OML-HN (1 μg) plus Poly(I:C). Three domain mutants of HPIV3-HN, the N-terminal region (1-190), the middle region (168-408) and C-terminal region (400-572) were synthesized using the wheat germ cell-free system (**Figure 4A** left) and protein production was confirmed by SDS-PAGE (**Figure 4A** right). Based on ELISA analysis, all of the serum samples contained HN-specific antibodies that had high reactivity to the N-terminal region (**Figure 4B**).

EFFECT OF OML-HN VACCINE ON HPIV3 INFECTION *IN VITRO*

We asked whether sera from the immunized mice could inhibit the HPIV3 infection of fibroblast cells. Infectious HPIV3 virions were pre-incubated with mouse serum harvested from three mice that were immunized with OML-HN plus Poly(I:C) and then used to infect MRC5 cells. Cellular HPIV3 mRNA was measured using quantitative reverse transcription PCR (qRT-PCR). The levels of HPIV3 mRNA were significantly reduced in cells pre-incubated with the immunized mouse serum compared to control serum that immunized with OML-empty (**Figure 4C**). These results indicate that the immunization with OML-HN plus Poly(I:C) induced serum antibodies that protect HPIV3 infection.

DISCUSSION

Herein, we developed a novel subunit vaccine against HPIV3-HN using OML and a mucosal adjuvant Poly(I:C). Consequently we

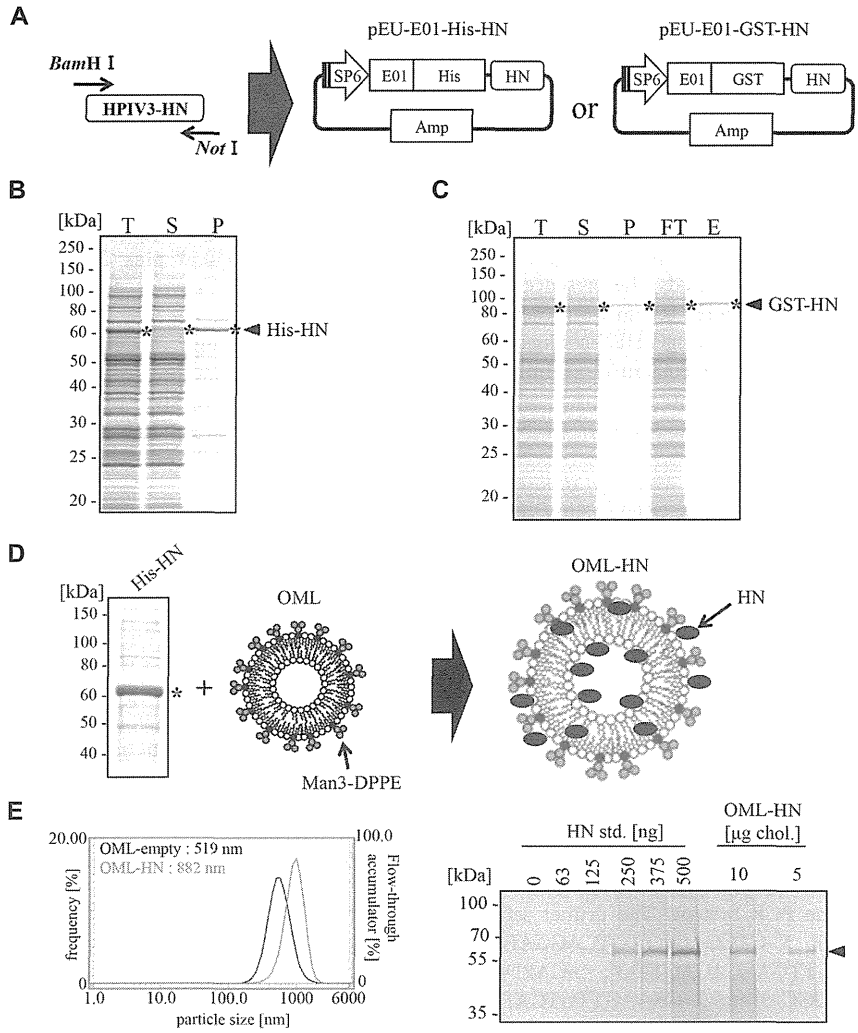

FIGURE 1 | Production of full-length HPIV3-HN and its encapsulation into OML. (A) Schematic representation of the expression vector for the wheat germ cell-free system. Full-length HN cDNA was subcloned into either pEU-His or pEU-GST vectors. **(B)** Expression and solubility of His-HN proteins that were synthesized using the wheat germ cell-free system. The translation reaction mixture (T) was subjected to centrifugation followed by the separation of the soluble supernatant (S) and insoluble precipitate (P) fractions. These samples were subjected to SDS-PAGE and visualized with Coomassie Brilliant Blue (CBB) staining. The single asterisk indicates the band of His-HN. **(C)** Purification of recombinant GST-tagged HPIV3-HN proteins that were synthesized using the wheat germ cell-free system. The translation mixture (T) was subjected to the separation into supernatant (S) and precipitate (P) fractions by centrifugation. GST-HN proteins were purified using glutathione sepharose bead and then resolved by SDS-PAGE and CBB staining. The single asterisk indicates the band of GST-HN. FT, Flow through fraction; E, elute fraction. **(D)** Schematic of the production of OML-encapsulated His-HN. The single asterisk indicates the band of His-HN. **(E)** The amount of encapsulated HN was quantitated by SDS-PAGE (right panel). The diameter of OML-HN or control OML were measured by dynamic light scattering particle size analyzer (left panel). The arrow indicates the band of His-HN.

successfully induced antigen-specific immunoglobulin G and A with the immunization of lower quantities of HN antigen via the nasal route. Furthermore, the immunized mouse serum exhibited the ability to suppress the virus infection in cell culture model. These results indicate that our newly developed OML vaccine could offer a powerful means to protect HPIV3 infection.

In our current study, we used the wheat germ cell-free protein production system to synthesize full-length HN protein as an antigen (Takai et al., 2010). In comparison to cell-mediated procedures such as *Escherichia coli* and baculovirus systems, the wheat germ cell-free system is beneficial for the rapid and efficient preparation of high-quality proteins (Endo and Sawasaki, 2006). Moreover, this cell-free system is suitable for the generation of toxic viral proteins for immunization and beneficial for the purification of naturally folded proteins, as well as scalability. This system, however, may not be cost-effective for preparing large

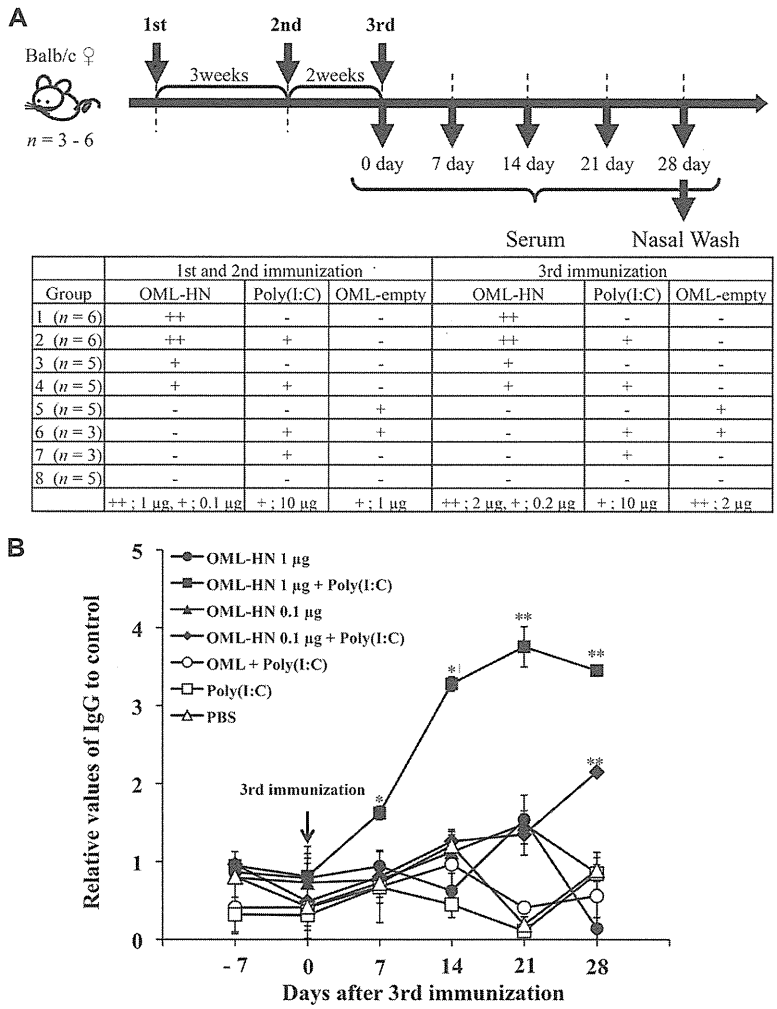

	1st and 2nd immunization			3rd immunization		
Group	OML-HN	Poly(I:C)	OML-empty	OML-HN	Poly(I:C)	OML-empty
1 ($n = 6$)	++	-	-	++	-	-
2 ($n = 6$)	++	+	-	++	+	-
3 ($n = 5$)	+	-	-	+	-	-
4 ($n = 5$)	+	+	-	+	+	-
5 ($n = 5$)	-	-	+	-	-	+
6 ($n = 3$)	-	+	+	-	+	+
7 ($n = 3$)	-	+	-	-	+	-
8 ($n = 5$)	-	-	-	-	-	-
	++ ; 1 μg, + ; 0.1 μg	+ ; 10 μg	+ ; 1 μg	++ ; 2 μg, + ; 0.2 μg	+ ; 10 μg	++ ; 2 μg

FIGURE 2 | Serum antibody responses in mice immunized with OML-HPIV3-HN. (A) Balb/c mice were immunized with the indicated antigens and/or adjuvant on days 0, 21, 35 as described in the Materials and Methods. Serum was collected from each mouse on days 7, 14, 21, and 28 after the third immunization. The bottom panel summarizes the time course for the immunizations. **(B)** HN-specific IgG in pooled serum from each group was measured by ELISA. Data represents the mean ± SE. (*t* test: $^{**}P < 0.01$, $^{*}P < 0.05$)

amounts of viral antigens for vaccine development. Therefore, efforts were made to reduce the amount of antigen needed vaccination. Herein, we utilized a OML and Poly(I:C) vaccination strategy in an attempt to reduce the amount of antigen required. OML is a lipid vesicle that has mannose on its surface, which aids in efficient targeting to APCs (Shimizu et al., 2007; Nishimura et al., 2013). In a previous report, antigenic proteins incorporated into OML were efficiently delivered to APCs via intranasal administration (Ishii and Kojima, 2010). In that report, intranasal administration of 5 μg ovalbumin (OVA) incorporated into OML four times effectively induced immune responses in mice (Ishii and Kojima, 2010). Poly(I:C) is a synthetic double-stranded RNA (dsRNA) molecule that induces effective mucosal immune responses by stimulating Toll-like receptor 3 (TLR3) as a molecular mimic of dsRNA, which is a byproduct of viral replication (Ichinohe et al., 2005; Hasegawa et al., 2009). The efficacy of nasal vaccines made of subunit proteins in the combination with mucosal adjuvants was demonstrated for influenza virus and RSV (Ichinohe et al., 2005; Hasegawa et al., 2009; Ainai et al., 2010; Kamphuis et al., 2013). We utilized a mucosal adjuvant Poly(I:C) to induce HN-specific antibodies in serum and nasal wash fluid through intranasal immunization with OML-HN. Using our vaccination strategy, we were able to decrease the amount of antigen required to 20% relative to previous reports (Mader et al., 2000; Ishii and Kojima, 2010).

The mucosa of respiratory tracts is the site of defense against virus infection since respiratory viruses attack and infect the respiratory mucosal tissues and cells (Tamura and Kurata, 2004). Mucosa is generally protected by mucin and defensin produced from goblet cells and Paneth cells. The TLR family members,

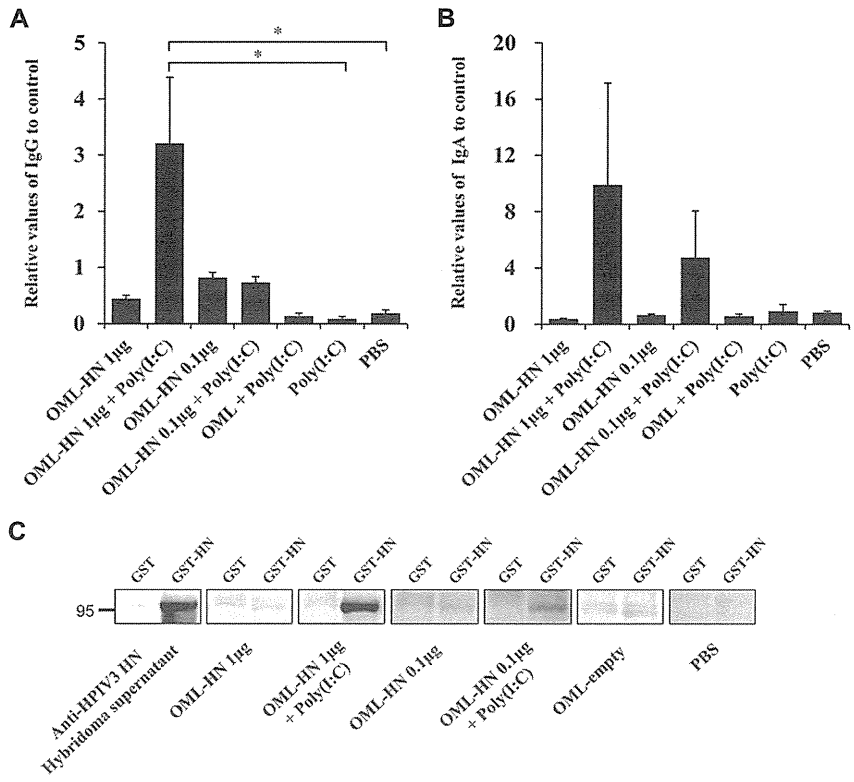

FIGURE 3 | Measurement of HPIV3-HN-specific serum IgG and nasal wash IgA. (A) The levels of HN-specific IgG in the serum of each immunized mouse on day 21 after the third immunization were determined by ELISA. **(B)** The levels of HN-specific IgA in nasal wash fluid on day 28 after the third immunization were determined by ELISA. Each bar represents the mean ± SE (*t* test: $*P < 0.05$). **(C)** Immunoblot analysis of recombinant HN proteins in mouse sera. Recombinant GST or GST-HN proteins were subjected to SDS-PAGE followed by the immunoblotting with the indicated serum.

TLR3, TLR7, TLR8, and TLR9 can recognize viral nucleotides and induces type I interferon (IFN-I) production if viruses intrude into tissues beyond the barrier. IFN-I activates the defense mechanism against virus by promoting the maturation of DCs and the induction of NK cells (Takeda et al., 2003; Akira et al., 2006). On the other hand, it is known that Microfold cells (M cells) promotes adherence and transport of antigens to APCs (Sato and Kiyono, 2012). M cells reside in the follicle-associated epithelium of Peyer's patches in the intestinal tract or nasal lymphoid tissue (NALT) of rodents in the upper respiratory tract, and plays a pivotal role in the induction of antigen-specific immunity (Nochi and Kiyono, 2006). The APCs promote adaptive immune responses by presenting antigens to naïve B cells and activate it to differentiate into antigen specific B cells. In the mucosa, secretory IgA is transported to mucosal surface by polymeric Ig receptor (pIgR) and the secreted IgA plays an important role in the protection of viral infection in the respiratory tract (Mostov and Deitcher, 1986). It is known that the intranasal immunization can activate mucosal immunity thereby enhancing the induction of mucosal IgA in addition to the generation of systemic IgG against viral antigen. Our current study employed OML as an effective tool to deliver the antigen to APCs and M cells in respiratory mucosa. A recent report demonstrated that OML-mediated intranasal immunization can efficiently induce Th2 cytokines such as IL-5 and IL-6 that eventually help produce secretory IgA in mucosal system in mouse model (Ishii and Kojima, 2010). We further combined OML with a mucosal adjuvant Poly(I:C) to facilitate the specific mucosal immunity against HPIV3-HN. Poly(I:C) has been shown to be an effective mucosal adjuvant stimulating TLR3 as a molecular mimic. A previous report indicated that a nasal influenza virus vaccine combined with Poly(I:C) synergistically induced IFN-1 and Th2 cytokine leading to an effective humoral immunity including secretory IgA in mucosa (Ichinohe et al., 2005). Our current study also demonstrated that the combinatory use of nasal vaccine with Poly(I:C) has a profound effect in inducing mucosal immunity against viral antigen.

Our newly developed OML-HN vaccine has several advantages as compared with previously developed vaccine methods including live attenuated vaccines. Although there is no practical prophylactic vaccine against HPIV3 infection, several previous studies have indicated that attenuated vaccines created by reducing the virulence of HPIV3 can indeed effectively induce the mucosal immunity when treated by intranasal administration (Karron et al., 2003). However, a major problem of these vaccines is their potential to cause a live infection in infants and immunocompromised hosts. Furthermore, there is a small risk of reversion to

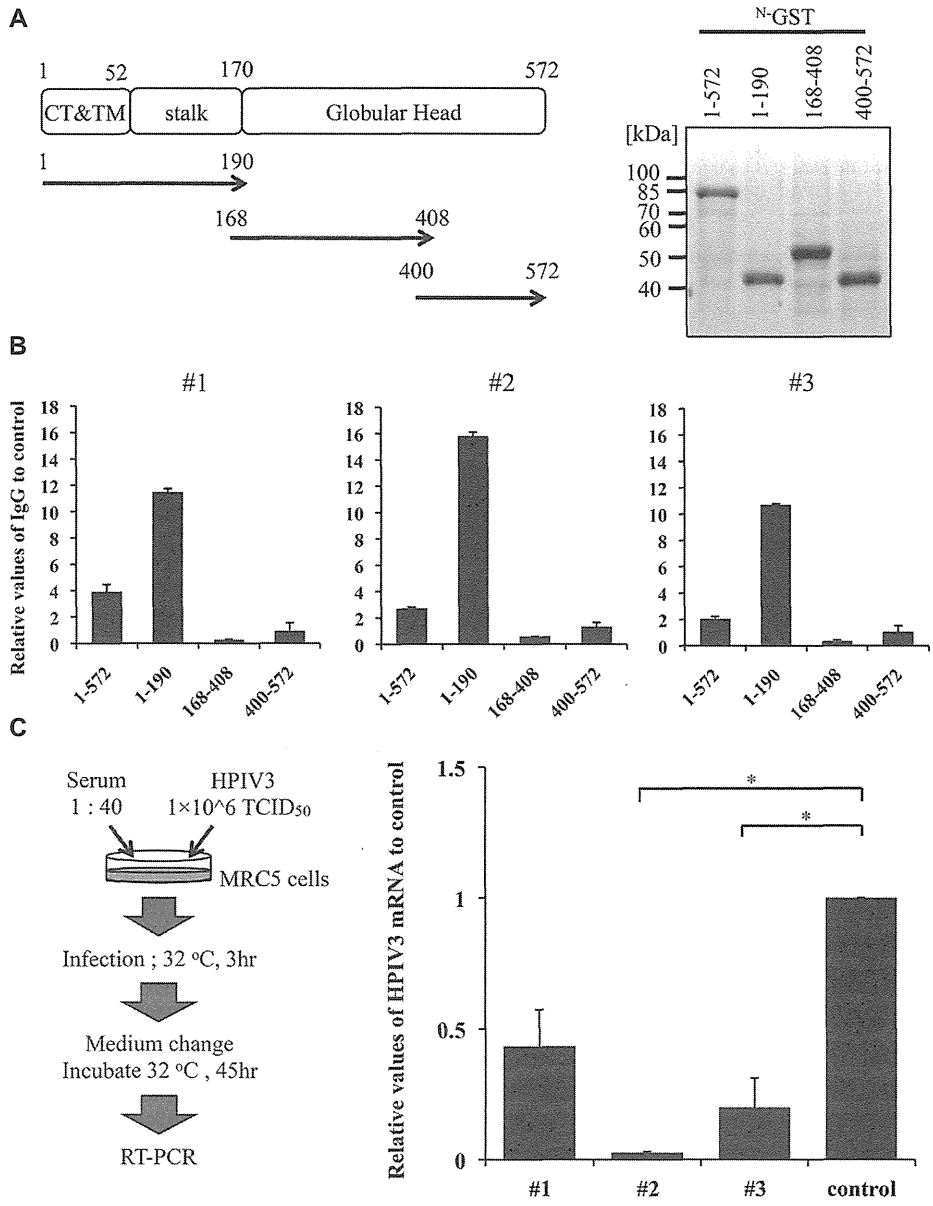

FIGURE 4 | Anti-infectious activity of mouse serum. (A,B) Epitope mapping of antibodies induced in the immunized mouse. We selected arbitrary three representative sera from mice immunized with OML-HN (1 μg) plus Poly(I:C) that exhibited the highest HN-specific IgG induction (#1–#3). The full-length and three deletion mutants of GST-HN were produced using the wheat germ cell-free system. These purified proteins were separated by SDS-PAGE and visualized using CBB staining **(A)**. Using the recombinant HN proteins, the target region of the three sera (#1–#3) was analyzed by ELISA **(B)**. **(C)** Schematic representation of the experimental procedure of infection-inhibitory assay (left panel). Immunized mouse sera (#1–#3) were tested for this assay. An OML-empty-treated mouse serum was used as a control. The anti-infection ability was measured using quantitative real-time PCR for HPIV3-HN mRNA. Each bar represents the mean ± SE of two independent experiments as normalized by control serum (*t* test: $^*P < 0.05$).

virulence by genetic mutations that results in the onset of severe disease. Therefore, it is desirable to develop a safer HPIV3 vaccine with lower risks of infection. On the other hand, intranasal subunit vaccines against HPIV3 have been demonstrated to be effective in animal models without the risk of viral replication and live infection. According to a report by Ray et al., the intranasal administration of HN and F proteins extracted from virions could induce significant anti-viral immunity in hamsters (Ray et al., 1988). However a drawback of subunit vaccines is their requirements for large amounts of antigens and concomitant high cost. Therefore, it is important to develop a cost-effective subunit vaccine that dispenses with substantial quantity of antigens. In order

to overcome this problem, we used OML and Poly (I:C) aiming for efficient vaccine delivery and immune response, respectively. Indeed, our current study demonstrated that a combination of OML-HN with poly(I:C) induced antigen-specific IgA and IgG by three times more than the immunization without poly(I:C). The safety in the use of either OML or poly(I:C) has been reported in previous studies. For OML-based vaccine, Fukasawa et al. have reported that OML has indeed no obvious toxicity and immunogenicity by itself (Fukasawa et al., 1998). Furthermore, Poly(I:C) has shown to be non-toxic as compared with conventional vaccine adjuvant such as cholera toxin subunit B (Ichinohe et al., 2005). However, further careful analysis should be necessary to validate the effectiveness and feasibility of our newly-developed vaccine strategy using virus infection models with multiple genotypes of HPIV3.

In our current study, we demonstrated that the OML-based vaccine incorporated with full-length HN protein induced IgG that targets the N-terminal region of HN protein. The N-terminal region of HN contains the stalk region while the C-terminal region contains the globular head domain. The stalk region of HN is known to play a crucial role in virion-host cell fusion via an interaction with F protein while the globular head binds sialic acid and neuraminidase (Moscona, 2005; Porotto et al., 2012). Although effective antigenic epitopes for HPIV vaccine remain elusive (Henrickson, 2003), a monoclonal antibody targeting the stalk region of HPIV2-HN has been shown to have a profound inhibitory activity against viral infection (Yuasa et al., 1995). Based on the observation, it seems that the antibodies induced by our vaccine system could also target the stalk region since they effectively blocked the viral infection in cell culture model. Further careful analysis will be required for the mapping of the epitope affecting virus infection in our current model.

In this study, we did not investigate other routes of antigen administration besides the intranasal route. However, previous studies have indicated that non-nasal immunization of HPIV3 components failed to prohibit the infection of HPIV3 in a cotton rat model. Indeed, the intramuscular immunization with HN and F recombinant proteins could not protect virus infection in upper respiratory tract although it had some effects on the protection of pneumonia and lower respiratory tract infection (Ambrose et al., 1991). It is generally believed that intranasal immunization has a great benefit for protecting virus infection itself by inducing antigen-specific secretory IgA in respiratory mucosa (Hirabayashi et al., 1990; Durrer et al., 2003). Our current study also confirmed this advantage of nasal vaccination where the OML-based nasal vaccine provides high performance for the induction of antigen-specific secretory IgA in nasal wash fluids. Therefore, intranasal administration of OML-based vaccine with poly(I:C) adjuvant could be an effective way of vaccination against respiratory viruses including HPIV3.

ACKNOWLEDGMENTS

We thank Drs. A Kudoh, A Ainai, and Y Sato for discussion and comments. This work was supported in part by grants from the Ministry of Education, Culture, Sports, Science and Technology of Japan and Respiratory Infection Disease Research Grants from The Ministry of Health Labour and Welfare of Japan to Akihide Ryo.

REFERENCES

Ainai, A., Ichinohe, T., Tamura, S., Kurata, T., Sata, T., Tashiro, M., et al. (2010). Zymosan enhances the mucosal adjuvant activity of poly(I:C) in a nasal influenza vaccine. *J. Med. Virol.* 82, 476–484. doi: 10.1002/jmv.21694

Akira, S., Uematsu, S., and Takeuchi, O. (2006). Pathogen recognition and innate immunity. *Cell* 124, 783–801. doi: 10.1016/j.cell.2006.02.015

Ambrose, M. W., Wyde, P. R., Ewasyshyn, M., Bonneau, A. M., Caplan, B., Meyer, H. L., et al. (1991). Evaluation of the immunogenicity and protective efficacy of a candidate parainfluenza virus type 3 subunit vaccine in cotton rats. *Vaccine* 9, 505–511. doi: 10.1016/0264-410X(91)90037-7

Belshe, R. B., Newman, F. K., Anderson, E. L., Wright, P. F., Karron, R. A., Tollefson, S., et al. (2004). Evaluation of combined live, attenuated respiratory syncytial virus and parainfluenza 3 virus vaccines in infants and young children. *J. Infect. Dis.* 190, 2096–2103. doi: 10.1086/425981

Brideau, R. J., Oien, N. L., Lehman, D. J., Homa, F. L., and Wathen, M. W. (1993). Protection of cotton rats against human parainfluenza virus type 3 by vaccination with a chimeric FHN subunit glycoprotein. *J. Gen. Virol.* 74, 471–477. doi: 10.1099/0022-1317-74-3-471

Counihan, M. E., Shay, D. K., Holman, R. C., Lowther, S. A., and Anderson, L. J. (2001). Human parainfluenza virus-associated hospitalizations among children less than five years of age in the United States. *Pediatr. Infect. Dis. J.* 20, 646–653. doi: 10.1097/00006454-200107000-00003

de Haan, A., Geerligs, H. J., Huchshorn, J. P., Van Scharrenburg, G. J., Palache, A. M., and Wilschut, J. (1995). Mucosal immunoadjuvant activity of liposomes: induction of systemic IgG and secretory IgA responses in mice by intranasal immunization with an influenza subunit vaccine and coadministered liposomes. *Vaccine* 13, 155–162. doi: 10.1016/0264-410X(95)93129-W

Durrer, P., Gluck, U., Spyr, C., Lang, A. B., Zurbriggen, R., Herzog, C., et al. (2003). Mucosal antibody response induced with a nasal virosome-based influenza vaccine. *Vaccine* 21, 4328–4334. doi: 10.1016/S0264-410X(03)00457-2

Endo, Y., and Sawasaki, T. (2006). Cell-free expression systems for eukaryotic protein production. *Curr. Opin. Biotechnol* 17, 373–380. doi: 10.1016/j.copbio.2006.06.009

Fukasawa, M., Shimizu, Y., Shikata, K., Nakata, M., Sakakibara, R., Yamamoto, N., et al. (1998). Liposome oligomannose-coated with neoglycolipid, a new candidate for a safe adjuvant for induction of CD8+ cytotoxic T lymphocytes. *FEBS Lett.* 441, 353–356. doi: 10.1016/S0014-5793(98)01577-4

Giddam, A. K., Zaman, M., Skwarczynski, M., and Toth, I. (2012). Liposome-based delivery system for vaccine candidates: constructing an effective formulation. *Nanomedicine (Lond.)* 7, 1877–1893. doi: 10.2217/nnm.12.157

Glezen, W. P., Frank, A. L., Taber, L. H., and Kasel, J. A. (1984). Parainfluenza virus type 3: seasonality and risk of infection and reinfection in young children. *J. Infect. Dis.* 150, 851–857. doi: 10.1093/infdis/150.6.851

Haller, A. A., Miller, T., Mitiku, M., and Coelingh, K. (2000). Expression of the surface glycoproteins of human parainfluenza virus type 3 by bovine parainfluenza virus type 3, a novel attenuated virus vaccine vector. *J. Virol.* 74, 11626–11635. doi: 10.1128/JVI.74.24.11626-11635.2000

Hasegawa, H., Ichinohe, T., Ainai, A., Tamura, S., and Kurata, T. (2009). Development of mucosal adjuvants for intranasal vaccine for H5N1 influenza viruses. *Ther. Clin. Risk Manag.* 5, 125–132. doi: 10.2147/TCRM.S3297

Henrickson, K. J. (2003). Parainfluenza viruses. *Clin. Microbiol. Rev.* 16, 242–264. doi: 10.1128/CMR.16.2.242-264.2003

Hirabayashi, Y., Kurata, H., Funato, H., Nagamine, T., Aizawa, C., Tamura, S., et al. (1990). Comparison of intranasal inoculation of influenza HA vaccine combined with cholera toxin B subunit with oral or parenteral vaccination. *Vaccine* 8, 243–248. doi: 10.1016/0264-410X(90)90053-O

Ichinohe, T., Watanabe, I., Ito, S., Fujii, H., Moriyama, M., Tamura, S., et al. (2005). Synthetic double-stranded RNA poly(I:C) combined with mucosal vaccine protects against influenza virus infection. *J. Virol.* 79, 2910–2919. doi: 10.1128/JVI.79.5.2910-2919.2005

Ishii, M., and Kojima, N. (2010). Mucosal adjuvant activity of oligomannose-coated liposomes for nasal immunization. *Glycoconj. J.* 27, 115–123. doi: 10.1007/s10719-009-9263-8

Kamphuis, T., Shafique, M., Meijerhof, T., Stegmann, T., Wilschut, J., and De Haan, A. (2013). Efficacy and safety of an intranasal virosomal respiratory syncytial virus vaccine adjuvanted with monophosphoryl lipid A in mice and cotton rats. *Vaccine* 31, 2169–2176. doi: 10.1016/j.vaccine.2013.02.043

Karron, R. A., Belshe, R. B., Wright, P. F., Thumar, B., Burns, B., Newman, F., et al. (2003). A live human parainfluenza type 3 virus vaccine is attenuated and immunogenic in young infants. *Pediatr. Infect. Dis. J.* 22, 394–405. doi: 10.1097/01.inf.0000066244.31769.83

Karron, R. A., Casey, R., Thumar, B., Surman, S., Murphy, B. R., Collins, P. L., et al. (2011). The cDNA-derived investigational human parainfluenza virus type 3 vaccine rcp45 is well tolerated, infectious, and immunogenic in infants and young children. *Pediatr. Infect. Dis. J.* 30, e186–e191. doi: 10.1097/INF.0b013e31822ea24f

Karron, R. A., Thumar, B., Schappell, E., Surman, S., Murphy, B. R., Collins, P. L., et al. (2012). Evaluation of two chimeric bovine-human parainfluenza virus type 3 vaccines in infants and young children. *Vaccine* 30, 3975–3981. doi: 10.1016/j.vaccine.2011.12.022

Mader, D., Huang, Y., Wang, C., Fraser, R., Issekutz, A. C., Stadnyk, A. W., et al. (2000). Liposome encapsulation of a soluble recombinant fragment of the respiratory syncytial virus (RSV) G protein enhances immune protection and reduces lung eosinophilia associated with virus challenge. *Vaccine* 18, 1110–1117. doi: 10.1016/S0264-410X(99)00373-4

Mason, J. N., Elbahesh, H., and Russell, C. J. (2013). Influence of antigen insertion site and vector dose on immunogenicity and protective capacity in Sendai virus-based human parainfluenza virus type 3 vaccines. *J. Virol.* 87, 5959–5969. doi: 10.1128/JVI.00227-13

Mizuta, K., Saitoh, M., Kobayashi, M., Tsukagoshi, H., Aoki, Y., Ikeda, T., et al. (2011). Detailed genetic analysis of hemagglutinin-neuraminidase glycoprotein gene in human parainfluenza virus type 1 isolates from patients with acute respiratory infection between 2002 and 2009 in Yamagata prefecture, Japan. *Virol. J.* 8, 533. doi: 10.1186/1743-422X-8-533

Morein, B., Sharp, M., Sundquist, B., and Simons, K. (1983). Protein subunit vaccines of parainfluenza type 3 virus: immunogenic effect in lambs and mice. *J. Gen. Virol.* 64, 1557–1569. doi: 10.1099/0022-1317-64-7-1557

Moscona, A. (2005). Entry of parainfluenza virus into cells as a target for interrupting childhood respiratory disease. *J. Clin. Invest.* 115, 1688–1698. doi: 10.1172/JCI25669

Mostov, K. E., and Deitcher, D. L. (1986). Polymeric immunoglobulin receptor expressed in MDCK cells transcytoses IgA. *Cell* 46, 613–621. doi: 10.1016/0092-8674(86)90887-1

Nishimura, M., Kohara, J., Kuroda, Y., Hiasa, J., Tanaka, S., Muroi, Y., et al. (2013). Oligomannose-coated liposome-entrapped dense granule protein 7 induces protective immune response to Neospora caninum in cattle. *Vaccine* 31, 3528–3535. doi: 10.1016/j.vaccine.2013.05.083

Nochi, T., and Kiyono, H. (2006). Innate immunity in the mucosal immune system. *Curr. Pharm. Des* 12, 4203–4213. doi: 10.2174/138161206778743457

Porotto, M., Palmer, S. G., Palermo, L. M., and Moscona, A. (2012). Mechanism of fusion triggering by human parainfluenza virus type III: communication between viral glycoproteins during entry. *J. Biol. Chem.* 287, 778–793. doi: 10.1074/jbc.M111.298059

Ray, R., Brown, V. E., and Compans, R. W. (1985). Glycoproteins of human parainfluenza virus type 3: characterization and evaluation as a subunit vaccine. *J. Infect. Dis.* 152, 1219–1230. doi: 10.1093/infdis/152.6.1219

Ray, R., Glaze, B. J., Moldoveanu, Z., and Compans, R. W. (1988). Intranasal immunization of hamsters with envelope glycoproteins of human parainfluenza virus type 3. *J. Infect. Dis.* 157, 648–654. doi: 10.1093/infdis/157.4.648

Sato, S., and Kiyono, H. (2012). The mucosal immune system of the respiratory tract. *Curr. Opin. Virol.* 2, 225–232. doi: 10.1016/j.coviro.2012.03.009

Schmidt, A. C. (2011). Progress in respiratory virus vaccine development. *Semin. Respir. Crit. Care Med.* 32, 527–540. doi: 10.1055/s-0031-1283289

Schmidt, A. C., Mcauliffe, J. M., Murphy, B. R., and Collins, P. L. (2001). Recombinant bovine/human parainfluenza virus type 3 (B/HPIV3) expressing the respiratory syncytial virus (RSV) G and F proteins can be used to achieve simultaneous mucosal immunization against RSV and HPIV3. *J. Virol.* 75, 4594–4603. doi: 10.1128/JVI.75.10.4594-4603.2001

Schmidt, A. C., Schaap-Nutt, A., Bartlett, E. J., Schomacker, H., Boonyaratanakornkit, J., Karron, R. A., et al. (2011). Progress in the development of human parainfluenza virus vaccines. *Expert. Rev. Respir. Med.* 5, 515–526. doi: 10.1586/ers.11.32

Shimizu, Y., Takagi, H., Nakayama, T., Yamakami, K., Tadakuma, T., Yokoyama, N., et al. (2007). Intraperitoneal immunization with oligomannose-coated liposome-entrapped soluble leishmanial antigen induces antigen-specific T-helper type immune response in BALB/c mice through uptake by peritoneal macrophages. *Parasite Immunol.* 29, 229–239. doi: 10.1111/j.1365-3024.2007.00937.x

Skiadopoulos, M. H., Surman, S., Tatem, J. M., Paschalis, M., Wu, S. L., Udem, S. A., et al. (1999). Identification of mutations contributing to the temperature-sensitive, cold-adapted, and attenuation phenotypes of the live-attenuated cold-passage 45 (cp45) human parainfluenza virus 3 candidate vaccine. *J. Virol.* 73, 1374–1381.

Takai, K., Sawasaki, T., and Endo, Y. (2010). Practical cell-free protein synthesis system using purified wheat embryos. *Nat Protoc.* 5, 227–238. doi: 10.1038/nprot.2009.207

Takeda, K., Kaisho, T., and Akira, S. (2003). Toll-like receptors. *Annu. Rev. Immunol.* 21, 335–376. doi: 10.1146/annurev.immunol.21.120601.141126

Tamura, S., and Kurata, T. (2004). Defense mechanisms against influenza virus infection in the respiratory tract mucosa. *Jpn. J. Infect. Dis.* 57, 236–247.

Yuasa, T., Kawano, M., Tabata, N., Nishio, M., Kusagawa, S., Komada, H., et al. (1995). A cell fusion-inhibiting monoclonal antibody binds to the presumed stalk domain of the human parainfluenza type 2 virus hemagglutinin-neuraminidase protein. *Virology* 206, 1117–1125. doi: 10.1006/viro.1995.1035

Conflict of Interest Statement: The authors, editor, and chief editor declare that while the authors Kyosuke Senchi, Satoko Matsunaga, Akihide Ryo, and the review editor Ichiro Aoki are currently employed by the same institution (Yokohama City University School of Medicine, Japan) and while Hirokazu Kimura and Hironori Sato are currently employed by the same institution (National Institute of Infectious Diseases, Japan) there has been no conflict of interest during the review and handling of this manuscript.

Received: 09 August 2013; paper pending published: 26 August 2013; accepted: 30 October 2013; published online: 26 November 2013.

Citation: Senchi K, Matsunaga S, Hasegawa H, Kimura H and Ryo A (2013) Development of oligomannose-coated liposome-based nasal vaccine against human parainfluenza virus type 3. Front. Microbiol. 4:346. doi: 10.3389/fmicb.2013.00346

This article was submitted to Virology, a section of the journal Frontiers in Microbiology.

Gold Nanoparticles as a Vaccine Platform: Influence of Size and Shape on Immunological Responses *in Vitro* and *in Vivo*

Kenichi Niikura,[†,*] Tatsuya Matsunaga,[‡] Tadaki Suzuki,[§] Shintaro Kobayashi,[⊥,∥] Hiroki Yamaguchi,[⊥,∥] Yasuko Orba,[⊥] Akira Kawaguchi,[§] Hideki Hasegawa,[§] Kiichi Kajino,[¶] Takafumi Ninomiya,[#] Kuniharu Ijiro,[†] and Hirofumi Sawa[⊥,∥]

[†]Research Institute for Electronic Science (RIES), Hokkaido University, N21W10, Sapporo 001-0021, Japan, [‡]Graduate School of Chemical Sciences and Engineering, Hokkaido University, Sapporo 060-8628, Japan, [§]Department of Pathology, National Institute of Infectious Diseases, Tokyo 162-8640, Japan, [⊥]Division of Molecular Pathobiology, Research Center for Zoonosis Control, Hokkaido University, Sapporo 001-0020, Japan, [∥]Global COE Program, Hokkaido University, Sapporo 060-0818, Japan, [¶]Division of Collaboration and Education, Research Center for Zoonosis Control, Hokkaido University, Sapporo 001-0020, Japan, and [#]Sapporo Medical University School of Medicine, Sapporo 060-8556, Japan

ABSTRACT This paper demonstrates how the shape and size of gold nanoparticles (AuNPs) affect immunological responses *in vivo* and *in vitro* for the production of antibodies for West Nile virus (WNV). We prepared spherical (20 and 40 nm in diameter), rod (40 × 10 nm), and cubic (40 × 40 × 40 nm) AuNPs as adjuvants and coated them with WNV envelope (E) protein. We measured anti-WNVE antibodies after inoculation of these WNVE-coated AuNPs (AuNP-Es) into mice. The 40 nm spherical AuNP-Es (Sphere40-Es) induced the highest level of WNVE-specific antibodies, while rod AuNP-Es (Rod-Es) induced only 50% of that of Sphere40-E. To examine the mechanisms of the shape-dependent WNVE antibody production, we next measured the efficiency of cellular uptake of AuNP-Es into RAW264.7 macrophage cells and bone-marrow-derived dendritic cells (BMDCs) and the subsequent cytokine secretion from BMDCs. The uptake of Rod-Es into the cells proceeded more efficiently than those of Sphere-Es or cubic WNVE-coated AuNPs (Cube-Es), suggesting that antibody production was not dependent on the uptake efficiency of the different AuNP-Es. Cytokine production from BMDCs treated with the AuNP-Es revealed that only Rod-E-treated cells produced significant levels of interleukin-1β (IL-1β) and interleukin-18 (IL-18), indicating that Rod-Es activated inflammasome-dependent cytokine secretion. Meanwhile, Sphere40-Es and Cube-Es both significantly induced inflammatory cytokine production, including tumor necrosis factor-α (TNF-α), IL-6, IL-12, and granulocyte macrophage colony-stimulating factor (GM-CSF). These results suggested that AuNPs are effective vaccine adjuvants and enhance the immune response *via* different cytokine pathways depending on their sizes and shapes.

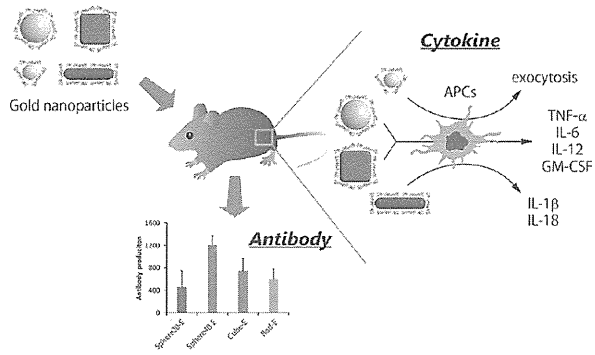

KEYWORDS: gold nanoparticle · vaccine · colloid · west nile virus · cytokine · antibody · shape dependence

Recent efforts to make effective and safe vaccines have focused on the development of subunit vaccines in which an antigen alone is linked to a strong immunogen, such as keyhole limpet hemocyanin (KLH) proteins.[1−3] However, issues remain regarding the use KLH as a vaccine platform. The antigen-KLH conjugate induces antibodies specific for both antigens and KLH, making multiple vaccinations inefficient due to the exclusion by KLH-specific antibodies.[4−6] In order to avoid antibody production against the platform materials, inorganic nanoparticles, in particular, gold, are strong candidates. In fact, gold nanoparticles (AuNPs) have already been used as antigen carriers for subunit vaccines without the production of anti-AuNP antibodies.[6] AuNPs have attracted attention as a nanomaterial in the biomedical

* Address correspondence to kniikura@poly.es.hokudai.ac.jp.

Received for review December 10, 2012 and accepted April 30, 2013.

Published online 10.1021/nn3057005

field due to their unique characteristics,[7−11] such as their biocompatibility[10] and easy fabrication in terms of size and shape.[12,13] Tohyama *et al.* first reported the production of antibodies in mice using glutamate-immobilized AuNPs.[14] Subsequently, the usefulness of AuNPs as an antigen carrier has been demonstrated for antigens derived from various viruses including influenza[15] and foot-and-mouth disease.[6,15] In these studies, conventional adjuvants, such as complete Freund's adjuvant or alum, which are used for enhanced induction of immunity, were coadministered with nanoparticle (NP) vaccines.

Recently, there have been a few reports that NPs alone can induce immunological responses, such as antibody and cytokine secretion.[16−18] Antigen-presenting cells (APCs), such as dendritic cells and macrophages, phagocytose external molecules/materials and stimulate lymphocytes and other immune cells by releasing chemical mediators, called cytokines, that initiate an adaptive immune response.[19,20] Hence, an understanding of the effects of nanoparticles on cytokine release is essential for their further application to vaccine adjuvants.[21] Tsai *et al.* reported that the expression levels of cytokines from macrophages after incubation with gold and silver nanoparticles were affected by the nanoparticle diameter.[22] Plebanski *et al.* reported that the size of antigen-immobilized polystyrene beads affected the type-1/type-2 cytokine balance.[17] These data suggest that nanoparticles of a suitable size could provide an effective adjuvant beyond their use as an antigen carrier.

Compared to effect of size, there are few reports on the effect of NP shape on the immunological response. Interestingly, Maysinger *et al.* reported the AuNP shape dependency of the inflammatory response in microglial cells.[23] For instance, the nanourchins increased interleukin-1α production, which is an inflammatory cytokine, but spherical and rod particles did not. These differences in cytokine production in response to nanoparticles of different shapes suggest a desirable alteration in immune response in accordance with changes in the shape of the nanoparticles used.

In this paper, we focused on the NP shape dependency of the immune response *in vivo* as well as *in vitro*. We prepared spherical (20 and 40 nm in diameter), rod (40 × 10 nm), and cubic (40 × 40 × 40 nm) nanoparticles. The nanoparticles were coated with West Nile virus envelope (WNVE) protein to produce 20 and 40 nm spherical (Sphere40-E, Sphere20-E), rod (Rod-E), and cubic (Cube-E) AuNP-Es. West Nile virus (WNV) is distributed over a wide geographical range including North America, Africa, Europe, and the Middle East; however, no practical vaccines for West Nile virus have been developed.[24] We chose these sizes because, in general, for mammalian cells, nanoparticles of 40−60 nm in diameter are known to be well-internalized into cells *via* the endocytotic pathway.[25−27] Further, the size of native WNV is also around 40 nm in diameter.[28] The levels of anti-WNVE antibody production in mice after vaccination with these particles were compared. We found that antibody production is significantly dependent on nanoparticle shape. In order to clarify the shape dependence *in vivo*, the cellular uptake of nanoparticles and subsequent cytokine production using RAW264.7 macrophages and murine bone-marrow-derived dendritic cells (BMDCs) were investigated. The correlations between antibody production, uptake level and cytokine production were discussed in regard to "nanoparticle shape".

RESULTS AND DISCUSSION

Characterization of WNVE-Coated AuNPs (AuNP-Es). Spherical, cubic, and rod AuNPs coated with cetyltrimethylammonium bromide (CTAB) were synthesized *via* a seeding growth method from chloroauric acid as reported previously with slight modifications.[13,29] Spherical AuNPs were synthesized in two sizes (20 and 40 nm in diameter; Figure 1A,B). The prepared AuNPs were then coated by an anionic polymer, poly(4-styrenesulfonic acid-*co*-maleic acid) (PSS-MA),[30] which can electrostatically attach the WNVE in the same orientation[31] as the envelope proteins of the native virus. Importantly, CTAB-originated cytotoxicity was drastically reduced by the PSS-MA coating (data not shown). WNVE, as an antigen, was conjugated with PSS-MA-coated AuNPs *via* an electrostatic interaction, and the resultant AuNP-E complexes were characterized as described below.

The physical characteristics of AuNP-E complexes are shown in Table 1. The shape and size of the synthesized AuNPs were confirmed by scanning transmission electron microscopy (STEM) and UV−vis absorption (Figure 1 and Supporting Information Figures S1 and S2). The diameters of the spherical AuNPs (Sphere20s and Sphere40s) were determined to be 19 ± 1.9 and 43 ± 3.3 nm, respectively (Figure 1A,B). The cubic AuNPs (Cubes) had an edge length of 41 ± 4.8 nm (Figure 1C). The rod AuNPs (Rods) were 36 ± 3.6 nm long and 10 ± 1.2 nm wide (aspect ratio = 3.6, Figure 1D). Surface modifications in each step were confirmed by changes of ζ-potential (Figure 1E). The ζ-potentials for all AuNPs changed from positive to negative (−65 to −22 mV) after PSS-MA coating and were slightly negative (−10 to −24 mV) after WNVE conjugation (Figure 1E). Each AuNP showed the same trend, and Rod showed the highest ζ-potential of −10 ± 0.3 mV.

In order to quantify the number of protein molecules on a single AuNP surface, WNVE molecules attached on the AuNPs were peeled off using sodium dodecyl sulfate (SDS) and the number of protein molecules was estimated by Western blotting (Table 1). The number of immobilized WNVE proteins per particle was 74 ± 4, 52 ± 6, and 46 ± 2 for Sphere40-Es, Cube-Es, and Rod-Es, respectively, so no large differences were observed between these similarly sized (~40 nm)

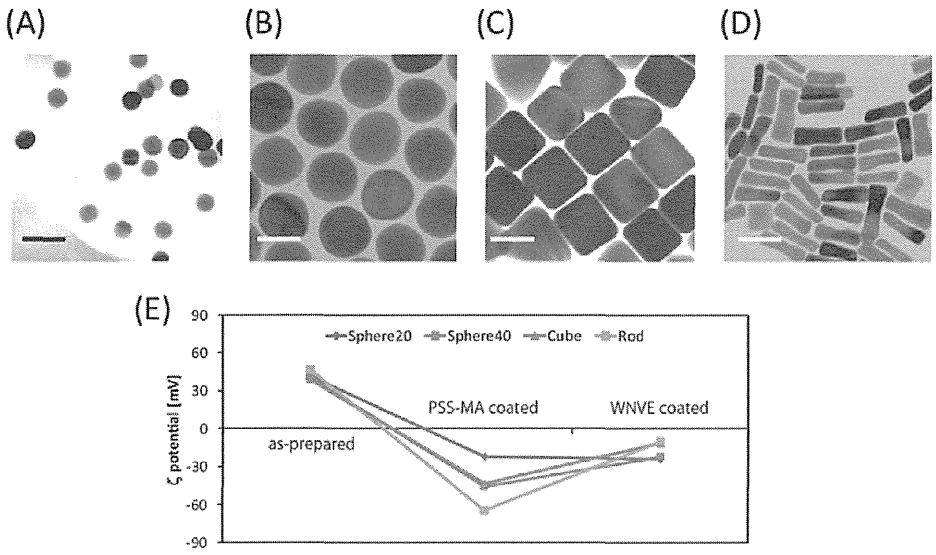

Figure 1. TEM images of as-prepared (A) Sphere20, (B) Sphere40, (C) Cube, and (D) Rod AuNPs. Scale bar represents 40 nm. (E) Zeta-potential (ζ) of AuNPs at each step of surface modification.

TABLE 1. Physical Characteristics of AuNP-E

	diameter (nm)[a]	λ_{max} (nm)	ζ-potential (mV)	number of protein/particle
Sphere20-E	19 ± 1.9	522	−24 ± 3	9.7 ± 3
Sphere40-E	43 ± 3.3	525	−23 ± 1	74 ± 4
Cube-E	41 ± 4.8	539	−11 ± 0.5	52 ± 6
Rod-E	(36 ± 3.6) × (10 ± 1.2)	516, 780	−9.9 ± 0.3	46 ± 2

[a] Determined from TEM images (means ± SD of 200 AuNPs).

particles. For Sphere20-Es, 9.7 ± 3 proteins were immobilized on the surface of a single nanoparticle. Immobilized WNVE molecules were not exchanged with serum protein during incubation for 2 h in a cell growth medium containing 10% fetal bovine serum (FBS) due to the slow exchange reaction rate of WNVE and serum protein (data not shown).

Colloidal Stability of AuNP-Es in a Biological Medium. As the proteins present in biological media interact with nanoparticles and form protein coronas around them,[32,33] shape of nanoparticles could affect protein corona formation so that the colloidal stability of nanoparticles in biological media could be the key feature in the immune response.[34−36] Therefore, the stability of each AuNP-Es in a serum medium (DMEM containing 10% FBS) was examined using dynamic light scattering (DLS) and UV−vis spectrometry (Figure 2). For Sphere40-Es, Sphere20-Es, and Cube-Es, 20−30 nm increases in the hydrodynamic diameter were observed during the initial 6 h of incubation, after which little further change was observed. In contrast, the hydrodynamic diameter, which corresponds to corona formation, was constant for Rod-Es during the initial 6 h period; however, the size suddenly increased after 6 h and reached a size 5 times larger than the original after incubation in serum for 24 h. The aggregation state of nanoparticles can be qualitatively evaluated by red shifts in the plasmon peak. While small shifts (2−6 nm) in the plasmon peak were observed for Sphere40-Es, Sphere20-Es, and Cube-Es during 24 h incubation in serum medium, a large shift (~20 nm) in the plasmon peak was observed for Rod-Es, supporting the aggregation of Rod-Es indicated by DLS. This means that, for Sphere40-Es, Sphere20-Es, and Cube-Es, incubation in serum induces the formation of a soft corona layer of serum proteins, affording colloidal stability to these AuNP-Es. In contrast, for Rod-Es, incubation in serum for 24 h resulted in only a small aggregation (less than 100 nm) of nanoparticles.

Antibody Responses in Mice Induced by AuNP-E Nanoparticles of Different Sizes and Shapes. The immunogenicity of the AuNP-E nanoparticles was examined in mouse experiments. Groups of 10 mice were intraperitoneally injected twice with 100 ng protein/animal/dose of AuNP-Es, WNVE protein that was not conjugated to AuNPs, or PBS as a negative control. WNVE-specific IgG titers in mice were determined by ELISA using WNVE protein as a coating antigen (Figure 3). The IgG specific to WNVE increased in mice immunized with all of the AuNP-Es. In particular, Sphere40-E showed the highest antibody induction of the four different AuNPs. However, WNVE protein without AuNPs induced almost no anti-WNVE IgG antibodies, similar to the PBS control. These results indicate that AuNPs can enhance antibody induction to the conjugated antigen, suggesting the AuNPs have an adjuvant effect. In addition, the adjuvant effects of AuNPs varied depending on their size and shape. Kojima *et al.* reported that West Nile virus-like particles of two different sizes, 20 and 40 nm, showed different levels of immunogenicity.[37] The larger virus-like particles induced a stronger immunological response than

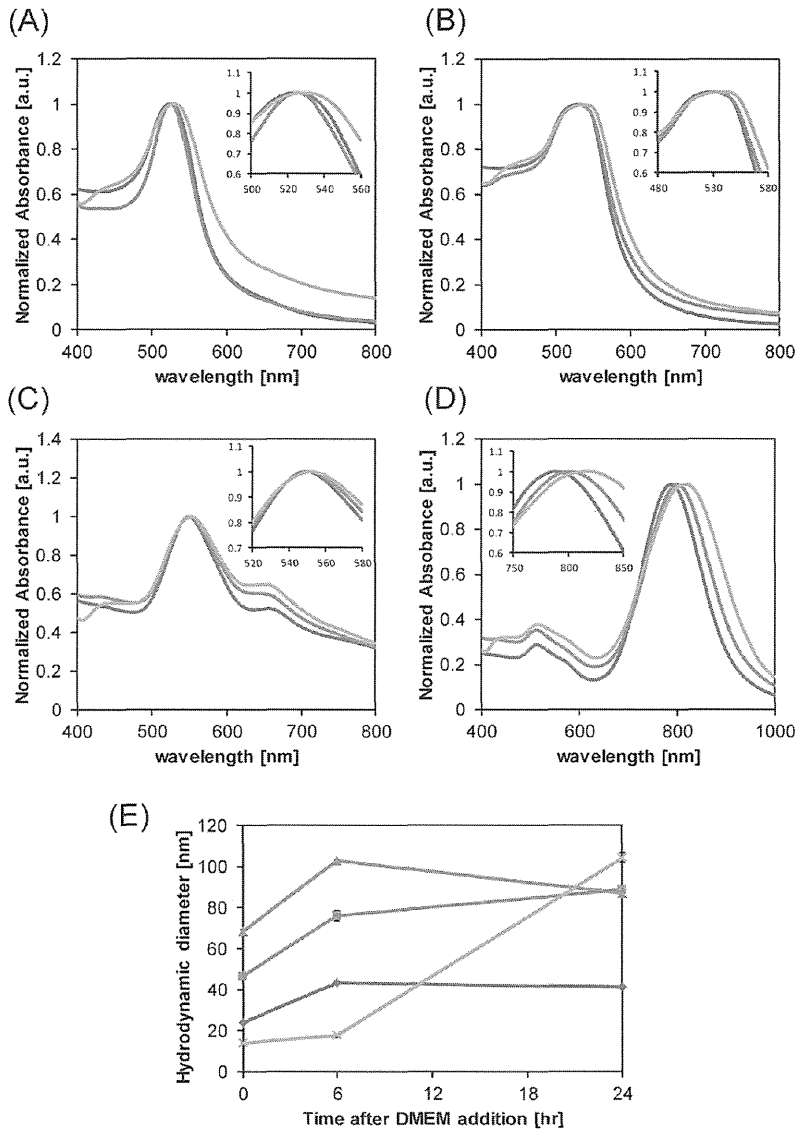

Figure 2. Red shift in absorbance spectra for (A) Sphere20, (B) Sphere40, (C) Cube, and (D) Rod nanoparticles on the addition of cell growth medium containing 10% FBS. Blue, red, and green lines indicate 0, 6, and 24 h after the addition of medium to the AuNP-Es, respectively. (E) Time-course change in hydrodynamic diameters determined by dynamic light scattering (DLS) after the addition of the medium to Sphere20-Es (blue), Sphere40-Es (red), Cube-Es (green), and Rod-Es (orange).

did the smaller ones in the same manner as our results for Sphere40-Es and Sphere20-Es. Notably, there were significant differences in antibody production between spherical, rod, and cubic NPs. The Sphere40-Es induced the highest level of WNVE-specific antibodies, while Rod-Es induced only 50% that of the Sphere40-Es.To explain the shape dependency of antibody production, we carried out *in vitro* studies using APCs based on the following two hypotheses. The first is that differences in the level of uptake of these NPs resulted in differences in the amount of antigen internalized into the APCs. The second is that cytokine production by the APCs is affected by the shape of the nanoparticles.

Comparison of the Cellular Uptakes of Sphere20-E, Sphere40-E, Cube-E, and Rod-E NPs into RAW264.7 Macrophages. At first, we examined the uptake level of the AuNP-Es to validate the first hypothesis using RAW264.7 cells, which are often used as a model for primary macrophages.[38] RAW264.7 cells were incubated with each AuNP-E at a concentration of 5×10^{10} NPs/mL in DMEM. The cytotoxicity of the AuNP-Es was evaluated using a cell-counting kit 8 (CCK-8) assay (Figure S3). None of the AuNP-Es led to obvious cell toxicity compared to the control cells at this concentration. The intracellular distributions of the AuNP-Es after incubation for 1.5 h were observed by confocal laser microscopy (CLMS) (Figure S4). In this experiment, proteins were labeled with Alexa Fluor 647 for their visualization. CLMS data demonstrate that all AuNP-Es were internalized into cells and were distributed outside the nucleus.

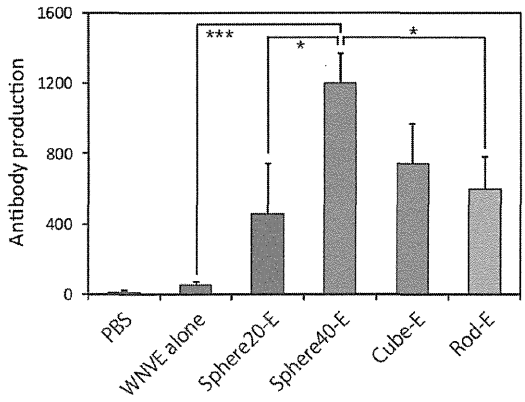

Figure 3. WNVE-specific IgG ELISA end point titers in mice immunized twice at 3 week intervals with 100 ng WNVE/animal/dose of AuNP-E. Antibody production was expressed as the reciprocal of the maximum dilution giving a greater absorbance than sera from PBS-immunized mice. Significant differences: *$p < 0.05$; ***$p < 0.001$ (means ± SEM, $n = 10$).

The level of cellular uptake of the AuNP-Es was detected by inductively coupled plasma atomic emission spectroscopy (ICP-AES) (Figure 4 and Figure S5). ICP-AES data indicate that the number of NPs in a single cell was 25, 7.1, 4.1, and 1.1×10^4 NPs/cell for Rod-Es, Sphere20-Es, Sphere40-Es, and Cube-Es, respectively (Figure 4A). Rod-shaped AuNPs were the most efficiently internalized among the tested particles, with 20% of the total NPs in the medium internalized within 1.5 h. On the contrary, the cubic AuNPs were internalized least efficiently, with only 1.3% of the added NPs entering the cells. The physicochemical properties of NPs, such as surface charge and surface area, are known to influence the cellular uptake of the NPs by macrophages.[39−41] The surface area of rods is similar to that of Sphere20s, and the surface charge of rods is similar to that of cubes. This means that the level of cellular uptake does not simply depend on surface area or charge, rather that shape is another important factor in determining the level of uptake. We also confirmed that AuNPs without a layer of WNVE proteins entered cells in a similar manner to WNVE-coated AuNPs (Figure S5). Frenkel *et al.* reported the effect of the shape of nanoparticles on passive endocytosis using MD simulations and found that the efficiency of endocytosis of spherocylindrical particles (similar in shape to our rods) was higher than that of spherical particles.[42] Ghandehari *et al.* compared the level of cellular uptake of PEGylated rod (10×45 nm) and spherical nanoparticles (50 nm in diameter) by RAW 264.7 macrophages.[41] They reported that the nanorods were taken up to a lesser extent than were the spherical nanoparticles based on the "weight of nanoparticles" in cells. These results seem to be inconsistent with our data. However, as each Sphere40 is 15-fold heavier than each rod, Figure 4A shows that the Sphere40s were more efficiently internalized into cells than rods when compared in terms of the weight of nanoparticles in a single cell. However, it should be noted that the number of internalized rods was 6 times higher than that of Sphere40s, meaning that Rod-Es can deliver WNVE antigens more efficiently into macrophages. Since Sphere40-Es induced the highest level of antibodies, the trend in antibody production shown in Figure 3 cannot be explained by the number of internalized AuNP-Es. This implies that there is another factor beyond the amount of antigen internalized.

Inflammasome Activation: Intracellular Distribution of AuNP-Es in RAW264.7 Cells. Next, we tested the second hypothesis that differences in the shape of the NPs induced differences in the level of cytokine production by APCs. First, we focused on the immunological response *via* inflammasomes, which are cytosolic molecular complexes that activate inflammatory caspase, cytokine IL-1β and IL-18, which promote inflammatory responses.[43,44] Inflammasomes are known to be activated on exposure to nanoparticles due to lysosomal damage, such as the rupture of lysosomes.[45−47] To examine this, the intracellular distribution of AuNP-Es in RAW264.7 cells was visualized by transmission electron microscopy (TEM) and CLMS (Figure S6). Regardless of the size and shape of the AuNPs, TEM images suggested that all AuNPs were taken up *via* the endocytotic pathway (Figure 4B−E). On the one hand, Sphere40-Es and Cube-Es mostly remained in the lysosome (Figure 4C,D), whereas Sphere20-Es and Rod-Es were capable of escaping from the lysosome into the cytosol (Figure 4B,E). CLMS images with lysosome staining by Lysotracker suggested the same trend as that observed in the TEM images (Figure S6). Nevertheless, CLMS images did show some release of Cube-Es from the lysosome, with a small number of Cube-Es also observed to be released in the TEM images (Figure S6E). These results are supported by the MD simulations reported by Frenkel *et al.*, in which small and nonspherical NPs were shown to easily escape from the lipid bilayer.[48] In addition, Sphere20-Es and Rod-Es were removed from cells by exocytosis after culturing for an additional 48 h (Figure 4F). These trends correlate with the lysosomal escape of AuNPs. This lysosomal escape means that Sphere20-Es and Rod-Es have potential cytotoxicity through the rupture of lysosomes and leakage of proteolytic lysosomal enzymes into the cytosol leading to inflammasome activation.

Inflammasome Activation in BMDCs after Exposure to AuNP-Es. IL-1β is a critical pro-inflammatory cytokine involved in the initiation of the innate immune response and regulation of adaptive immunity.[49] The maturation of this cytokine is tightly regulated by the NLRP3 inflammasome.[50] In recent years, there have been a few reports indicating that NPs stimulate NLRP3 inflammasome formation and that the stimulation efficacy depends on the size and surface chemical properties of the NPs.[45,46] Thus, the production of

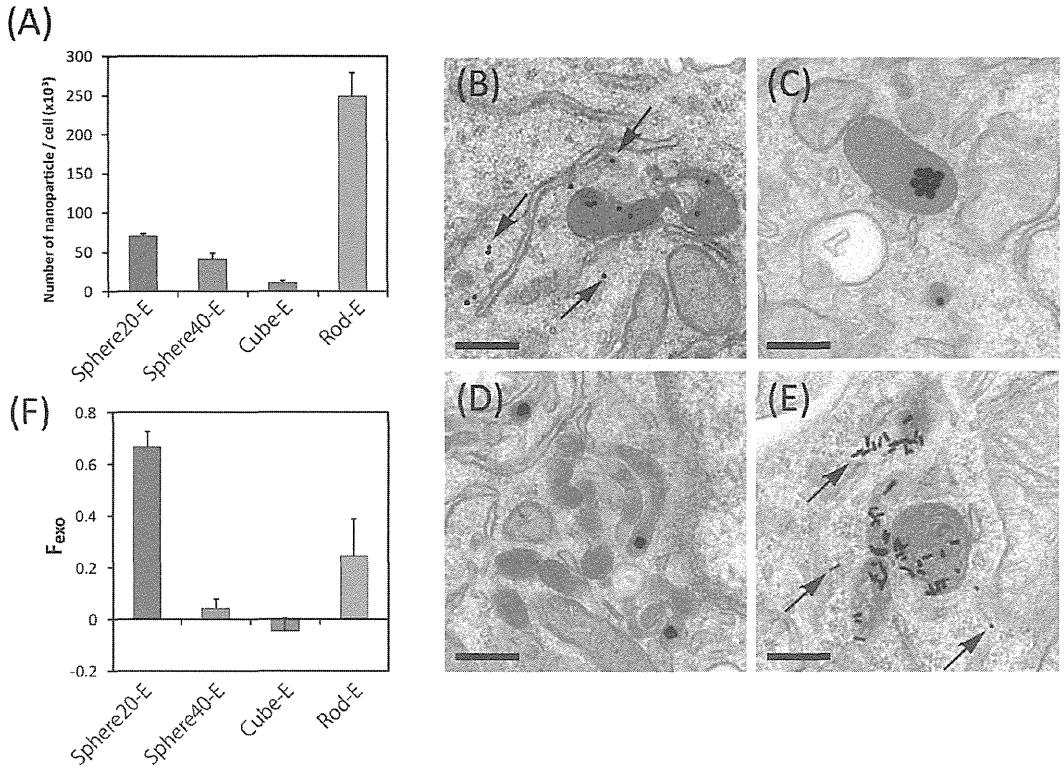

Figure 4. (A) Uptake of AuNP-E by RAW264.7 cells determined from ICP-AES (mean ± SEM, n = 3). TEM images of RAW264.7 cells treated with 2 mg/mL AuNP-Esfor 3 h; (B) Sphere20-E, (C) Sphere40-E, (D) Cube-E, and (E) Rod-E. Arrows indicate AuNP-E in the cytosol. Scale bar represents 300 nm. (F) Exocytotic level of AuNP-Es 48 h after exposure to AuNP-E for 1.5 h. $F_{exo} = N_{out}/N_0$, where N_{out} is the number of NPs exocytosed from the cells and N_0 is the number of NPs internalized before exocytosis (means ± SEM, n = 3).[22]

IL-1β and IL-18 in dendritic cells (DCs) was investigated by ELISA in order to reveal whether the shape-dependent antibody production originated from shape-dependent inflammasome activation or not.

BMDCs were incubated with AuNP-Es at various concentrations, from 2 to 10 μg/mL, for 24 h. CLMS images are shown in Figure 5 (enlarged images in Figure S7). As with RAW264.7 macrophages, AuNP-Es were internalized into cells and distributed outside the nucleus. The black areas within the cells in the DIC images represent internalized AuNP-Es, as the fluorescence from the dye-conjugated AuNP-Es (shown in red in Figure 5) corresponded to these black areas. According to the DIC images, a large number of Rod-Es were taken up, again as seen with RAW264.7 cells. ICP-AES data also supported the significant internalization of rods into the cells (Figure S8).

Cytotoxicity and cytokine production in BMDCs after exposure to AuNP-Es for 24 h in the presence of 50 ng/mL lipopolysaccharide (LPS) is shown in Figure 6. Aluminum potassium sulfate (alum) was used as a positive control for the observation of inflammasome activation.[51,52] LPS increases the amount of pro-IL-1β and pro-IL-18, the immature state of IL-1β and IL-18, in cells.[53] Cytotoxicity occurred in cells treated with Rod-Es at a concentration of 10 μg/mL, although WNVE alone or other AuNP-Es exhibited no cytotoxicity (Figure 6A). IL-1β and IL-18 levels were assessed in the culture supernatants of BMDCs after nanoparticle treatment by ELISA (Figure 6B,C). ELISA results indicated that only Rod-Es evoked IL-1β and IL-18 expression (752 ± 50 and 64 ± 0.8 pg/mL, respectively), while other AuNP-Es or WNVE alone did not. The cytokine production level correlated with the cytotoxicity of Rod-Es. Simmet *et al.* reported that cationic polystyrene nanoparticles induce lysosomal rupture followed by a cytotoxic effect and NLRP3 inflammasome activation.[45] Our rod-shaped AuNPs exhibited lysosomal escape to the cytosol (Figure 4E), and this could be similarly regarded as lysosomal rupture. Although Sphere20-Es can escape from lysosome similarly to Rod-Es, inflammasome activation was not observed. This suggests that the efficiency of internalization of AuNP-Es is one of the important factors to induce the inflammasome-mediated immune response. The cytotoxicity derived from the efficient internalization of Rod-Es and subsequent lysosomal rupture it thought to lead to inflammasome activation with IL-1β and IL-18 secretion. However, this AuNP-E-induced antibody production cannot be fully explained by inflammasome activation as efficient antibody production was also observed for Sphere40-Es and Cube-Es.

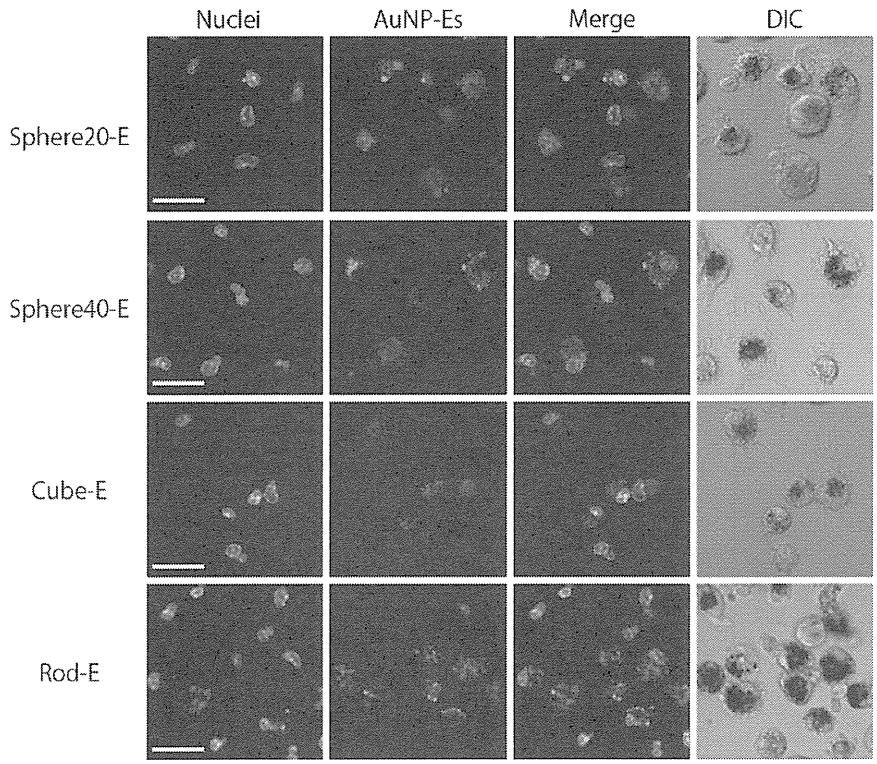

Figure 5. CLMS images of BMDCs treated with 10 μg/mL Alexa Fluor 647-labeled AuNP-Es for 24 h. Nuclei were stained by Hoechst for 30 min (green). Scale bar represents 20 μm.

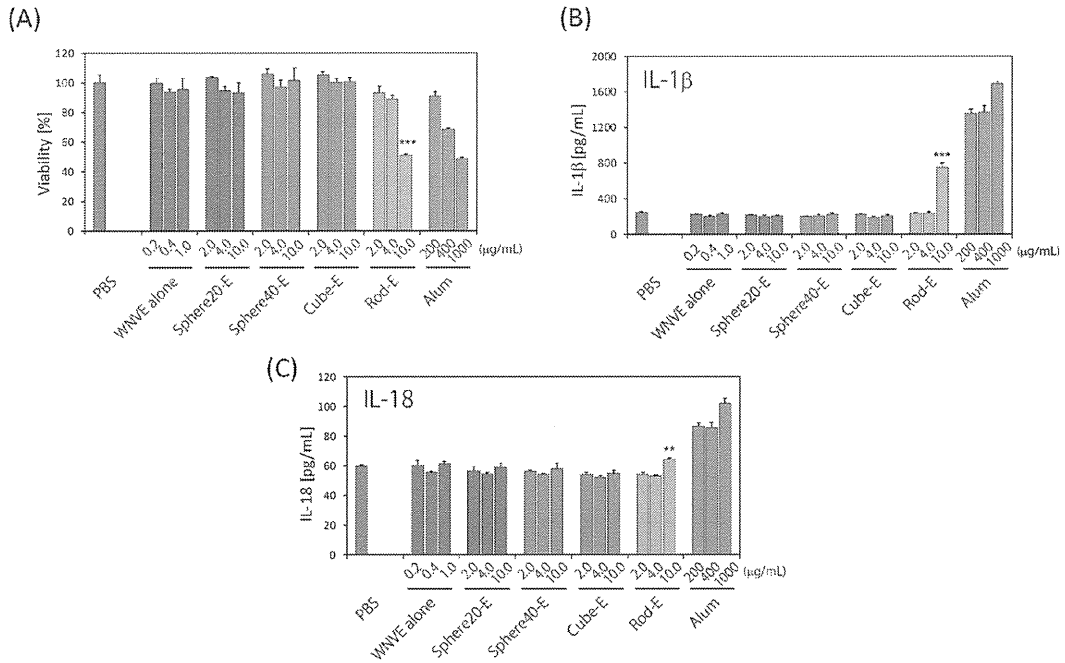

Figure 6. (A) Cytotoxicity of AuNP-Es to BMDCs at various concentrations after incubation for 24 h. (B) IL-1β and (C) IL-18 secretion from BMDCs as an indication of inflammasome activation. Significant differences: $^{**}p < 0.01$; $^{***}p < 0.001$ *vs* control (means ± SEM, $n = 3$).

Thus, there is a possibility that APCs recognize the shape of the nanoparticles and induce different cytokines for Sphere40-Es and Cube-Es through non-inflammasome pathway.

Inflammatory Cytokine Secretion from BMDCs after Exposure to AuNP-Es. One of the most important cytokines in the innate and adaptive immune systems is tumor necrosis factor-α (TNF-α), which is a pro-inflammatory cytokine

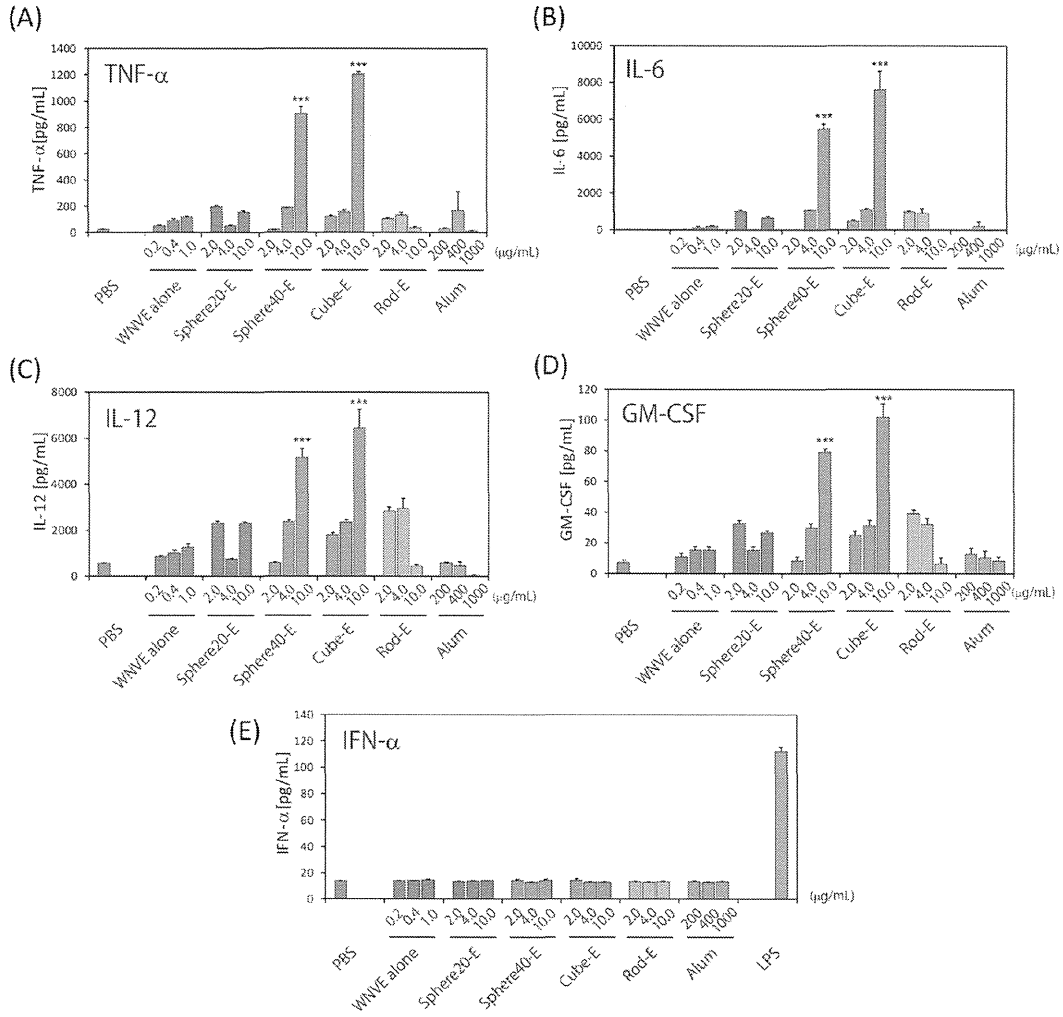

Figure 7. (A) TNF-α, (B) IL-6, (C) IL-12, (D) GM-CSF, and (E) IFN-α secretion from BMDCs treated with AuNP-Es at various concentrations. LPS was used as positive control for IFN-α (50 ng/mL for 3 h, red bar). Significant differences: ***$p < 0.001$ *vs* control (means ± SEM, $n = 3$).

mainly produced by T cells and APCs, such as dendritic cells and macrophages.[54] Importantly, this cytokine is not induced *via* the inflammasome-mediated immune response.[45,55] We examined TNF-α induction from BMDCs after exposure to AuNP-Es (Figure 7A). Sphere40-E and Cube-E NPs induced significantly higher levels of TNF-α (906 ± 50 and 1204 ± 20 pg/mL, respectively) than the other AuNP-Es tested (55−191 pg/mL). We confirmed that the alum adjuvant, which activates the inflammasome-mediated immune response, did not induce TNF-α (16−172 pg/mL). Interestingly, Rod-Es did not induce TNF-α secretion even though the uptake level was markedly higher than those of the other AuNP-Es. Therefore, for the induction of TNF-α, the shape of the AuNP-Es as well as their size is an important factor in the adjuvant function of AuNPs. In addition to TNF-α, induction of other inflammatory cytokines, IL-6, IL-12, and GM-CSF, was also investigated. The induction of IL-6, IL-12, and GM-CSF from BMDCs after treatment with AuNP-Es showed similar trends to that of TNF-α, and only both Sphere40-Es and Cube-Es induced the production of these cytokines (Figure 7B−D). On the contrary, no AuNPs induced interferon-α (IFN-α), which is known to interfere with viral replication in uninfected cells by activating NK cells and macrophages.[56] These data suggest that Sphere40-Es and Cube-Es induce antibodies by the induction of inflammatory cytokines, although these cytokines are different from those induced by Rod-Es. Rod-Es appear to induce antibody production through the inflammasome-mediated pathway (Figure 6). Our *in vitro* experiments clearly demonstrate that AuNP-Es can induce the production of different kinds of cytokines at different levels from dendritic cells in a shape-dependent manner.

Influence of the Physicochemical Parameters of AuNP-Es on Antibody Production and Cytokine Secretion. Although immune responses are also dependent on the pharmacokinetic aspects of the adjuvants *in vivo*, the